# Passivating electron-selective contacts for silicon solar cells based on an a-Si

Received: 30 October 2017 | Revised: 4 April 2018 | Accepted: 25 April 2018

DOI: 10.1002/pip.3023

RESEARCH ARTICLE

WILEY PROGRESS IN PHOTOVOLTAICS

# Passivating electron-selective contacts for silicon solar cells based on an a-Si:H/$TiO_x$ stack and a low work function metal

Jinyoun Cho[1,2] | Jimmy Melskens[3] | Maarten Debucquoy[2] | Maria Recamán Payo[2] | Shruti Jambaldinni[2] | Twan Bearda[2] | Ivan Gordon[2] | Jozef Szlufcik[2] | W.M.M. Kessels[3] | Jef Poortmans[1,2,4,5]

[1] ESAT Department, K.U. Leuven, Leuven 3001, Belgium

[2] imec, Kapeldreef 75, Leuven 3001, Belgium

[3] Department of Applied Physics, Eindhoven University of Technology, P.O. Box 513, 5600 MB Eindhoven, The Netherlands

[4] University Hasselt, Martelarenlaan 42, Hasselt 3500, Belgium

[5] EnergyVille, Thor Park 8310, Genk B-3600, Belgium

**Correspondence**
Jinyoun Cho, ESAT Department, K.U. Leuven, Leuven 3001, Belgium.
Email: jinyoun.cho@imec.be

**Funding information**
imec, Interuniversity Microelectronics Center, Belgium

## Abstract

In this work, the ATOM (intrinsic a-Si:H/$TiO_x$/low work function metal) structure is investigated to realize high-performance passivating electron-selective contacts for crystalline silicon solar cells. The absence of a highly doped Si region in this contact structure is meant to reduce the optoelectrical losses. We show that a low contact resistivity ($\rho_c$) can be obtained by the combined effect of a low work function metal, such as calcium (Φ 2.9 eV), and Fermi-level depinning in the metal-insulator-semiconductor contact structure (where in our case $TiO_x$ acts as the insulator on the intrinsic a-Si:H passivating layer). $TiO_x$ grown by ALD is effective to achieve not only a low $\rho_c$ but also good passivation properties. As an electron contact in silicon heterojunction solar cells, inserting interfacial $TiO_x$ at the i-a-Si:H/Ca interface significantly enhances the solar cell conversion efficiency. Consequently, the champion solar cell with the ATOM contact achieves a $V_{OC}$ of 711 mV, FF of 72.9%, $J_{SC}$ of 35.1 mA/cm$^2$, and an efficiency of 18.2%. The achievement of a high $V_{OC}$ and reasonable FF without the need for a highly doped Si layer serves as a valuable proof of concept for future developments on passivating electron-selective contacts using this structure.

**KEYWORDS**

carrier-selective, electron-selective, heterojunction, passivating contact, $TiO_x$, calcium, low work function metal

## 1 | INTRODUCTION

Industrial crystalline silicon solar cells (eg, passivated emitter rear totally diffused (PERT) cells, passivated emitter and rear contact (PERC) cells, or silicon heterojunction solar (SHJ) cells) use highly doped silicon layers.[1-4] The high doping concentration of these $n^+$ or $p^+$ silicon layers is very effective to lower the contact resistivity ($\rho_c$). However, heavy doping can induce parasitic absorption, Auger recombination, and Shockley-Read-Hall recombination.[5,6] Carrier-selective contacts without the use of highly doped silicon layers are getting attention to avoid these disadvantages.[7,8] However, a lowly doped silicon surface typically results in a high $\rho_c$.

Based on the Schottky-Mott rule,[9,10] when a metal work function is lower than the work function of a semiconductor, the band of the semiconductor near the metal-semiconductor (MS) interface should move downwards (forming an accumulation contact for electrons). Accordingly, many groups have aimed to reach a low $\rho_c$ for electron-selective contacts on n-type-based c-Si solar cells using low work function metals either individually[11,12] or in combination with other materials such as alkaline earth metal fluorides.[13,14] However, the main challenge of these approaches is that the penetration of the metal wave function into the semiconductor overlaps with surface states in the semiconductor energy band gap[15] resulting in metal Fermi-level ($E_{F,metal}$) pinning.[16] Therefore, the promised gain of the low work function is not fully realized, and a non-negligible Schottky energy barrier can still be formed at the interfaces with c-Si or a-Si:H.[17-19]

  

As an alternative, a metal-insulator-semiconductor (MIS) contact can mitigate the $E_{F,metal}$ pinning due to the reduction of surface states or dipoles at the interfaces of the contact.[20-23] In addition, when using low doping concentrations, it has been shown that an MIS contact can outperform the contact resistivity of an MS contact.[24,25] In the MIS structure, the thickness of the insulator is a critical parameter to obtain low $\rho_c$: the thicker the insulator layer is, the larger the reduction in the $E_{F,metal}$ pinning but also the larger the resistance for the carrier transport through the insulator itself. The position of the energy bands of the dielectric also plays an important role in this resistance. In this respect, $TiO_x$ stands out as a good candidate because it has a suitable band structure for electron-selective contacts: a small $E_C$ offset and a large $E_V$ offset relative to c-Si.[26]

For the aforementioned reasons, MIS contacts including $TiO_x$ layers with a typical thickness below 2 nm have been intensively studied in the field of CMOS[24,25,27-29] to achieve the lowest possible $\rho_c$ by mitigating $E_{F,metal}$ pinning. In silicon solar cells, solar cell efficiencies of above 20% have been successfully shown based on a slightly thicker $TiO_x$ layer of 3.5 nm which was subjected to a forming gas annealing treatment at 350°C.[30-32] When it is aimed to realize silicon solar cells that do not include highly doped silicon regions, a low-temperature process at or below 200°C is still required to be compatible with the fabrication of hole-selective contacts based on high work function transition metal oxides.[33-39] Therefore, electron-selective contacts with an intrinsic a-Si:H/$TiO_x$ stack have been researched because of good chemical passivation of i-a-Si:H, but a high contact resistivity for i-a-Si:H/$TiO_x$ likely limited the reported cell efficiencies.[40,41] In our previous work,[42] we demonstrated the ATOM (intrinsic a-Si:H/$TiO_x$/low work function metal) contact which achieves a reduction of 2 orders of magnitudes in $\rho_c$ by combining merits of a MIS contact and a low work function metal. Furthermore, the process temperature was below 200°C for the layers in the contact structure. However, the experiments performed to quantify the recombination losses clearly showed a higher dark saturation current density at the metalized area ($J_{0,metal}$) for the ATOM contacts adopting e-beam evaporated $TiO_x$ when compared to the contacts without $TiO_x$. It is believed that the a-Si:H passivation quality was degraded by e-beam radiation damages during the evaporation.[43,44]

In this work, ATOM contacts involving $TiO_x$ layers fabricated by atomic layer deposition (ALD) are evaluated in $\rho_c$ and $J_0$ to assess their potential in a passivating electron-selective contact. Finally, the ATOM contact structure with $TiO_x$ is integrated in heterojunction solar cells and compared to a classical SHJ solar cell.

## 2 | CHARACTERIZATION OF ATOM TEST STRUCTURES

### 2.1 | Preparation of test structures

Mirror polished n-type FZ-Si wafers (3 Ω cm, 200-µm thickness) were used to evaluate $\rho_c$ and the contact passivation quality. After HF:HCl cleaning, 8-nm-thick intrinsic a-Si:H (i-a-Si:H) layers were deposited on both sides of the substrate by plasma-enhanced chemical vapor deposition (PECVD) at temperatures below 200°C in an AK1000 Inline system of MicroSystems. Wafers were diced into squares of 54 × 54 $mm^2$ (for the determination of $J_0$) and 30 × 30 $mm^2$ (for the determination of $\rho_c$). After HF dip, on top of the i-a-Si:H layers, $TiO_x$ layers of 2 nm were deposited on both sides of the substrate by ALD (Oxford Instruments FlexAL, UK). For the ALD-$TiO_x$ process, titanium tetra-isopropoxide (TTIP) and $H_2O$ were used as Ti precursor and oxidant, respectively, and the substrate temperature was set to 200°C.

For the measurement of $J_0$, thin blanket layers of 4-nm-thick Ca and 6-nm-thick Al were deposited by thermal evaporation (Angstrom Engineering, USA) on the rear side of the substrate (see Figure 1A, B). The metal layer thickness was monitored using a quartz sensor in the evaporation tool. These metal layers were kept thin and were deposited only on the rear side to allow a quasi-steady-state photoconductance (QSSPC) measurement[45] with illumination from the front. The metal layer needs to be thin enough to achieve sufficiently low conductivities for the QSSPC measurement while thick enough to show metal-induced effects on the passivation. The metal thickness of a few Angstroms is sufficient to allow for a metal-induced effect to the band structure at the contact region.[46] Moreover, to avoid the nonconformal coating of metals and complete oxidation of Al, a few nanometers can be adequate.[47,48] A similar methodology to extract $J_{0,metal}$ have been previously reported in the literature.[49-51]

The QSSPC measurement was carried out before and after the thermal evaporation of the Ca/Al stack (see Figure 1A, B). This allowed us to calculate the $J_0$ of the complete ATOM stack based on implied $V_{OC}$ with a $J_{SC}$ of 36 mA/$cm^2$ (typical $J_{SC}$ of our SHJ solar cells), $kT/q$ = 25.9 mV, and $J_{0,bulk}$ = 0 fA/$cm^2$ (high-quality FZ-Si wafers).

Before Ca/Al evaporation, $J_{0,front}$ is calculated based on the symmetry of the structures. After Ca/Al deposition (see Figure 1B), $J_{0,rear\ Ca/Al}$ is determined by subtracting $J_{0,front}$, which was already measured before Ca/Al evaporation, from $J_{0,total,\ after\ Ca/Al}$. Assuming the same $J_{0,front}$ before and after Ca/Al evaporation is an acceptable approximation for these contact structures, as during Ca/Al thermal evaporation, the wafer temperature does not exceed 40°C and no process damage is generated because no plasma or e-beam is used.

For the measurement of $\rho_c$, 100 nm Ca and 200 nm Al were thermally evaporated through a shadow mask, yielding circular contacts with different diameters (200-600 µm) (see Figure 1C). The values of $\rho_c$ were extracted using the 2-contact 2-terminal method.[42,52] Consequently, the measured $\rho_c$ includes the $\rho_c$ contribution of all contact layers, as well as the resistive contributions of the bulk of these layers (i-a-Si:H/$TiO_x$/Ca/Al).

Samples for additional analysis were prepared using the same process as the $\rho_c$ samples based on double side chemically polished n-type Cz-Si wafers (3.7 Ω cm, 180-µm thickness). The nanoscale layer structure and the chemical distribution were further investigated by means of transmission electron microscopy (TEM) and energy-dispersive X-ray spectroscopy (EDX) measurements.

### 2.2 | Results of test structures

As shown in Table 1, no process damage of a-Si:H is observed after ALD-$TiO_x$ deposition, in contrast to the e-beam evaporated $TiO_x$ in our previous study[42] (note that all $TiO_x$ layer in this study were deposited using ALD). $J_0$ and $J_{0,metal}$ of the i-a-Si:H/$TiO_x$ structure exhibit

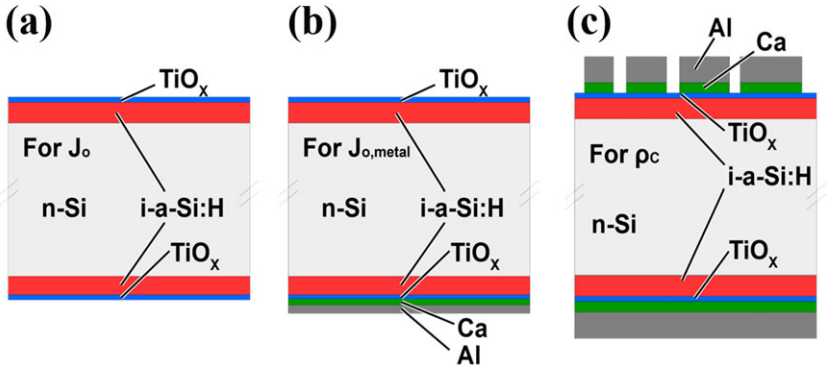


**FIGURE 1** Schematic of the sample structures to determine: (A) $J_0$, (B) $J_{0,metal}$, and (C) $\rho_c$ [Colour figure can be viewed at wileyonlinelibrary.com]

**TABLE 1** $J_0$ and contact resistivity comparison between contacts with/without $TiO_x$ layer

| Contact Structure | $J_0$ (fA/cm$^2$) | $\rho_c$ (average ± standard deviation) (Ω cm$^2$) |
|---|---|---|
| i-a-Si:H | 12.6 | |
| i-a-Si:H/Ca/Al | 17.4 | 8.2 ± 1.9 |
| i-a-Si:H/ALD-$TiO_x$ | 12.6 | |
| i-a-Si:H/ALD-$TiO_x$/Ca/Al (ATOM) | 13.4 | 1.5 ± 0.4 × $10^{-2}$ |

values similar to the structure without ALD-$TiO_x$, which means that neither the deposition of the $TiO_x$ layer nor the subsequent metallization results in significant damage to the passivation quality that is provided by the a-Si:H layer. A significant reduction of about 2 orders of magnitude in $\rho_c$ was achieved by the interfacial $TiO_x$, which illustrates that the presence of a $TiO_x$ layer induces Fermi-level depinning on the a-Si:H surface. As can be seen in Figure 2, the contact type is also changed from a Schottky contact to an Ohmic contact.

The features of the ATOM contact structures with $TiO_x$ were characterized by TEM and EDX and are shown in Figure 3. The rough c-Si/a-Si:H interface is because of a phase transition region of a few

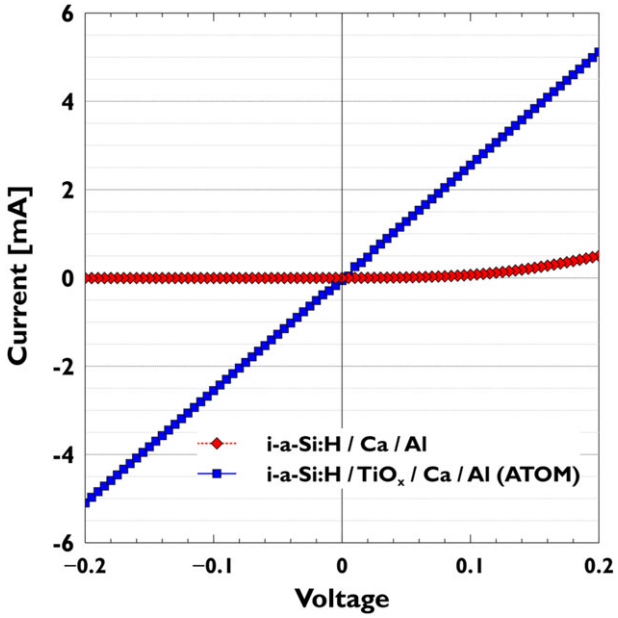


**FIGURE 2** Dark IV curve comparison between i-a-Si:H/Ca/Al and ATOM contact [Colour figure can be viewed at wileyonlinelibrary.com]

nanometers from crystalline to fully amorphous.[53,54] The $TiO_x$ layer, of which the thickness is around 2 nm, was deposited uniformly on the i-a-Si:H surface, showing no isolated islands. A closed $TiO_x$ layer is important to achieve $E_{F,metal}$ depinning, and a uniform $TiO_x$ layer thickness with an amorphous phase is required for homogeneous surface passivation.[55] Furthermore, an interfacial amorphous $SiO_x$ layer can be found in the EDX image between the i-a-Si:H and the $TiO_x$ layers (see Figure 3A). This interfacial $SiO_x$ may have a potentially positive impact on the passivation properties of the ATOM contact structure. According to Kita et al,[56] a dipole can be generated by oxygen movement resulting from a charge imbalance at the $SiO_x$/$TiO_x$ interface, which produces a downward band bending at the contact (see Figure 4B) which is beneficial in passivating electron-selective contacts.

After Ca/Al evaporation, the a-Si:H passivation layer preserves the original amorphous phase in both cases with and without $TiO_x$ in Figure 3C and in Supporting Information Figure S1. Moreover, Al on Ca formed a stack with a clear interface between Ca and Al (see Figure 3D).

Based on previous work,[42,57] it can be speculated that Ca diffused into the $TiO_x$ layer without any additional annealing. This in-diffusion of Ca within the $TiO_x$ layer may work as a dopant in the $TiO_x$, which results in lowering the conduction band of $TiO_x$.[58] Alternatively, it can be imagined that Ca also induces the formation of defects in the $TiO_x$ layer, especially when Ca is not active as a dopant. This could lead to enhanced trap-assisted transport that also lowers $\rho_c$. Furthermore, oxygen vacancies can be generated by oxygen extraction from the $TiO_x$ layer by Ca or Al metal.[31,57,59] It implies that the oxygen vacancies of $TiO_x$, interfacial $SiO_x$, and likely Ca in-diffusion possibly have a positive impact on increasing the major carrier conductivity and thus a reduction in $\rho_c$.

The energy band structures of the i-a-Si:H/Ca/Al and ATOM contact are illustrated in Figure 4. It is based on an effective Schottky energy barrier height ($\Phi_{B,eff}$), the layer stacks depicted in Figure 3, and the energy band of amorphous $SiO_x$.[60] Additionally, the movement of oxygen at the a-$SiO_x$/$TiO_x$ interface induces a dipole (negatively charged at $SiO_x$ side and positively charged at $TiO_x$ side from the interface).[56]

Allen et al calculated the $\Phi_{B,eff}$ based on $\rho_c$ using Equation (1) in thermionic emission condition.[11,61]

$$\rho_c = \left(k/qA^{**}T\right)\exp\left(\phi_{B,eff}/kT\right) \quad (1)$$

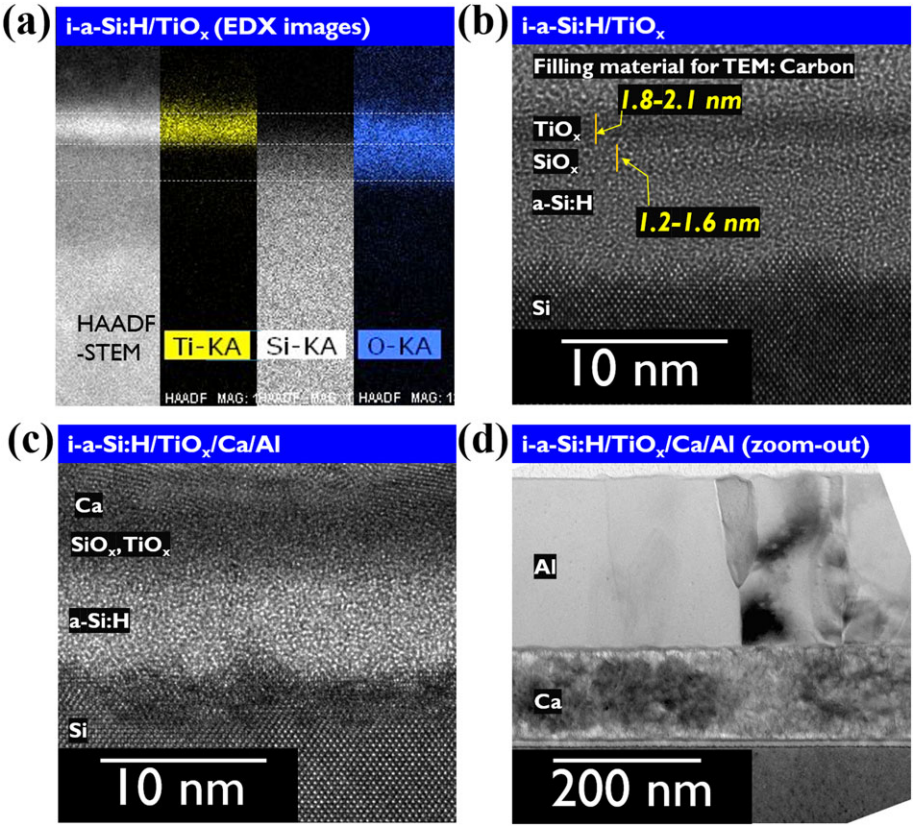


**FIGURE 3** TEM cross-sectional images for ATOM contact structures using $TiO_x$ deposited by ALD. In particular, EDX images of Ti, Si, and O are shown in (A), TEM images before Ca/Al evaporation in (B), and TEM images after Ca/Al evaporation with high magnification (C) and with low magnification (D) [Colour figure can be viewed at wileyonlinelibrary.com]

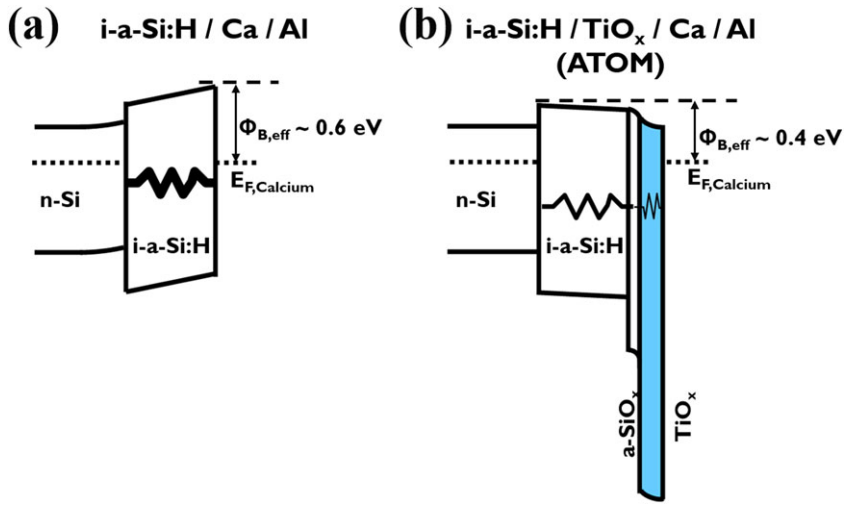


**FIGURE 4** Schematic band diagram of i-a-Si:H/Ca/Al and the ATOM contact structures based on effective Schottky energy barrier height, metal Fermi-level pinning, and a dipole at the $SiO_x/TiO_x$ interface. A, Ca layer induces upward band bending because of $E_{F,metal}$ pinning on the a-Si:H layer. B, The ATOM contact band structure includes an additional $TiO_x$ layer that induces Fermi-level depinning and hence enables a lower Schottky energy barrier [Colour figure can be viewed at wileyonlinelibrary.com]

where $A^{**}$ is the reduced effective Richardson constant (110 A/cm$^2$/K$^2$[262]), $k$ is the Boltzmann constant, and $\Phi_{B,eff}$ is the effective Schottky energy barrier at the contact. When this methodology is applied, the extracted $\Phi_{B,eff}$ on the i-a-Si:H layer is 0.6 eV for Ca and 0.4 eV for the ATOM contact. A significant change of the electron conductivity at the contact is resulting from this difference in barrier height, and $\Phi_{B,eff}$ of the ATOM contact is comparable to that of a n-Si/Ca/Al contact.[11] Temperature-dependent $\rho_c$ measurements could provide more detailed information about the barrier height, although they were not part of this study.

## 3 | SOLAR CELLS

### 3.1 | Solar cell preparation

Our ATOM contact was applied to 2-side contacted SHJ cells. The schematic cell structures are shown in Figure 5. All the cell structures investigated had the same hole-selective contact approach featuring the stack i/p-a-Si:H/ITO/Ag on the front side. On the rear side, different stacks were applied: i-a-Si:H/Ca/Al and i-a-Si:H/ALD-$TiO_x$/Ca/Al as highly doped Si layer free electron-selective passivating contact

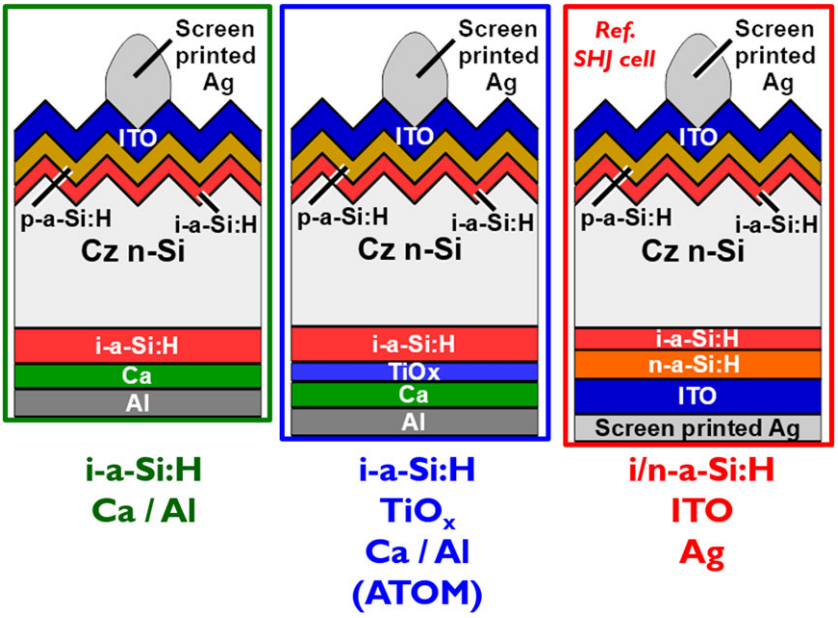


**FIGURE 5** Schematic cross-sectional structures for the different solar cells with candidate electron-selective contacts [Colour figure can be viewed at wileyonlinelibrary.com]

structures. As a reference contact, i/n-a-Si:H/ITO/Ag, which is commonly used in a classical SHJ cell, was applied.

To fabricate these solar cells, n-type Cz-Si wafers (3.2 Ω cm, 165-μm thickness) with a textured front side and a chemically polished rear side were used. After HF:HCl:$O_3$ and HF:HCl cleaning,[63] the i/p-a-Si:H stack was deposited on the textured front side. Subsequently, after a short HF cleaning, i-a-Si:H and n-a-Si:H layers with thicknesses of 4 and of 8 nm, respectively, were deposited by plasma-enhanced chemical vapor deposition (PECVD) for the reference sample, while 8 nm of i-a-Si:H was deposited on the other samples. For the SHJ cell,

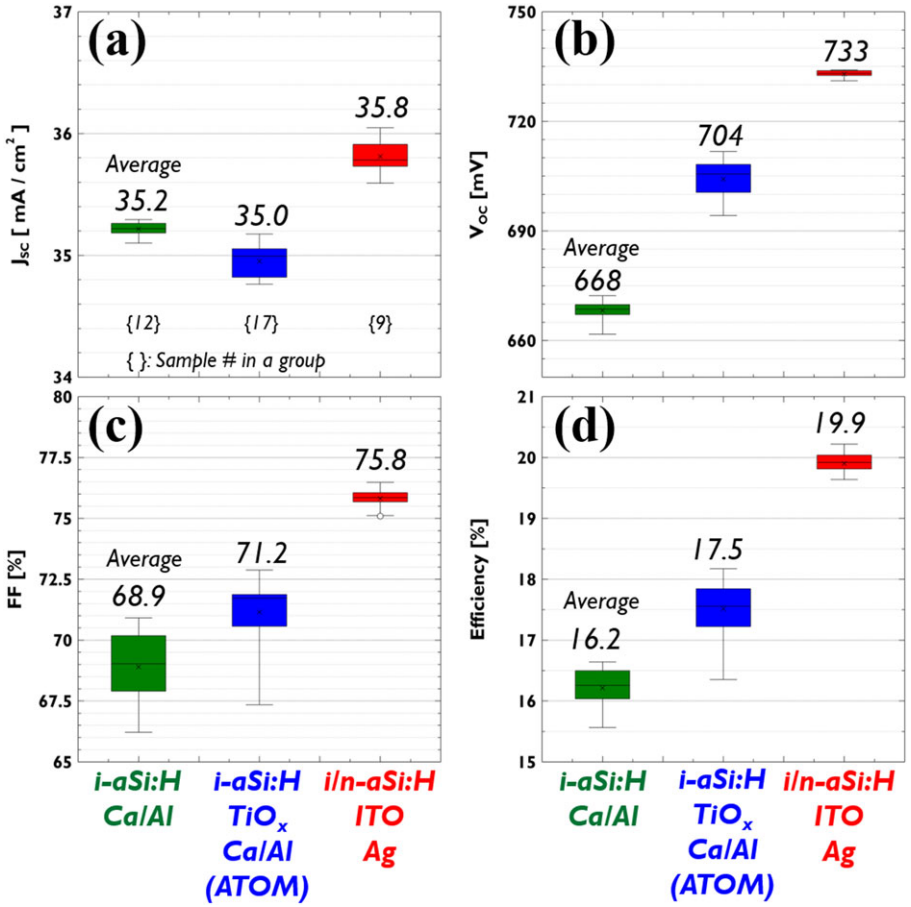


**FIGURE 6** Effect of candidate electron-selective contact structures on the light IV parameters. A, $J_{SC}$. B, $V_{OC}$. C, FF. D, Efficiency. The numbers in the box plot are the average external parameters of the solar cells in that group, while the sample quantity of each group is indicated in (A) with braces ({}) [Colour figure can be viewed at wileyonlinelibrary.com]

a 4-nm-thick i-a-Si:H layer leads to the best cell results. For the other cells, 8-nm-thick i-a-Si:H was applied as this resulted in the best passivation quality without n-a-Si:H, as has been demonstrated previously.[42] After HF dip, the $TiO_x$ layer was deposited by ALD to obtain a layer thickness of 2 nm for the samples with the i-a-Si:H/$TiO_x$/Ca/Al structure. After ITO sputtering, Ag fingers (100 μm wide, 17 μm high) and full area Ag (thickness of 17 μm) were printed on the front and rear sides of the reference cells, while this was only done on the front side of the other samples. Next, a belt furnace annealing at 175°C was performed to sinter the Ag contacts. In all samples but the reference SHJ cells, the rear metallization was completed with Al evaporation which was directly performed after Ca evaporation without breaking the vacuum. As the final step, the wafers were diced into solar cells of 5 × 5 $cm^2$.

Light IV characterization was conducted with an aperture opening of the same size as the active cell area of 4 × 4 $cm^2$ under calibrated illumination (AM 1.5, 1000 W/$m^2$ at 25°C). External quantum efficiency (EQE) and reflectance were measured in the same tool (PV-Tools LOANA, Germany) using a large beam size of 1.5 × 1.5 $cm^2$. Therefore, the EQE and reflectance results include the shading and reflecting effects of the metal grid.

## 3.2 | Solar cell results

The light IV parameters of the silicon solar cells with the different candidates for electron-selective contacts are shown in Figure 6 and Table 2. The IV curves of champion cells are found in Supporting Information Figure S2. The $J_{SC}$ values of all solar cells appear to be rather low, most likely caused by parasitic absorption in the ITO and the i/p-a-Si:H stack on the front side of the cells. More specifically, the average $J_{SC}$ of the solar cells with and the cells without $TiO_x$ are similar (see Figure 6A) while the reference cell shows a somewhat higher $J_{SC}$. $V_{OC}$ and FF are strongly dependent on the applied rear contact structure. ATOM contact which includes $TiO_x$, an average $V_{OC}$ enhancement of 36 mV, and an average FF improvement of 2.3%$_{abs}$ are achieved with respect to i-a-Si:H/Ca/Al contacted solar cells. The champion cell is a device with a $TiO_x$ layer showing a $V_{OC}$ of 711 mV. However, all cell parameters are still higher for the reference SHJ solar cells compared to the other cell structures, which will be discussed further at the end of this section.

To improve the understanding of the differences in $J_{SC}$, the EQE and reflectance curves were measured. As can be seen in Figure 7, much parasitic aborption in the front stack is inferred by low EQE response in short wavelengths. Moreover, the solar cell with the ATOM contact shows a similar EQE at longer wavelengths compared to the other candidate electron-selective contacts except for the reference SHJ contact. In comparison to the i-a-Si:H/Ca/Al contacted solar cell, the lower $J_{SC}$ of the solar cell with the ATOM contact structure is caused by a lower EQE at short wavelengths. An unintentional variation in front ITO thickness seems to play a role, which can be recognized by the peak shift of the reflectance at shorter wavelengths.

**TABLE 2** Light IV parameters of the champion cells within the different contact groups

| Candidate Electron-Selective Contact Structure | $J_{SC}$ (mA/$cm^2$) | $V_{OC}$ (mV) | FF (%) | η (%) |
|---|---|---|---|---|
| i-a-Si:H/Ca/Al | 35.2 | 666.3 | 70.9 | 16.6 |
| i-a-Si:H/$TiO_x$/Ca/Al (ATOM) | 35.1 | 710.8 | 72.9 | 18.2 |
| i/n-a-Si:H/ITO/Ag | 36.0 | 734.0 | 76.4 | 20.2 |

The active area and the aperture opening area: 16 $cm^2$.

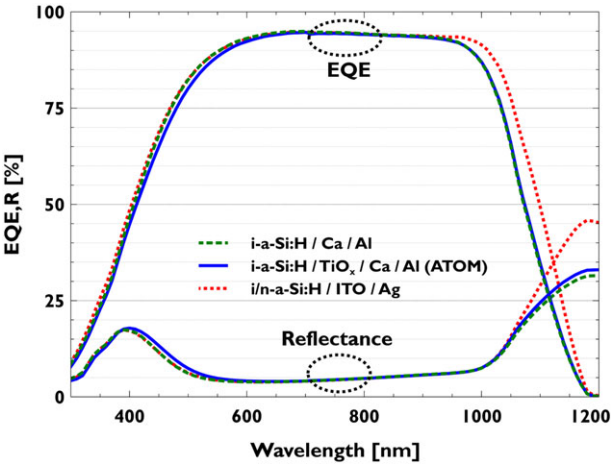


**FIGURE 7** EQE and reflectance for the best cells of the various candidate electron-selective contact structures [Colour figure can be viewed at wileyonlinelibrary.com]

At long wavelengths, there is virtually no difference between the cell with the i-a-Si:H/Ca/Al contact and the cell with the i-a-Si:H/$TiO_x$/Ca/Al (ATOM) contact. This indicates that the amount of parasitic absorption occurring in substoichiometric $TiO_x$[64] is negligible. The differences with the other cells at long wavelengths can be explained by the impact of the specific metal layout on the rear reflectance (see Figure 7). According to Allen et al,[11] the reflectance of the Ca/Al stack is lower than that for both Al and Ag. Furthermore, as shown in Supporting Information Figure S3 and Table S1, changing the metal from Ag to Ca/Al on i/n-a-Si:H/ITO reduces EQE and reflectance in the long wavelength range, similar to the result of the i-a-Si:H/Ca/Al contacted solar cell, while it does not change $V_{OC}$ and FF. Although the high EQE at longer wavelengths for the reference cell is partially because of the superior rear surface passivation quality, most of the $J_{SC}$ improvement is caused by the higher reflectance of Ag. For these reasons, strontium (Sr) and ytterbium (Yb) can be good alternatives to calcium (Ca) because of their superior reflectance properties, although still lower than Al.[65-67]

To further assess the contact performance and the $V_{OC}$ values of the solar cells, Suns$V_{OC}$ measurements have been conducted (see Figure 8). For the solar cells with i-a-Si:H/Ca/Al rear contacts, a bend (dashed circle areas in Figure 8) can be observed in the Suns$V_{OC}$ curve above 1 sun illumination intensity. This phenomenon occurs when $\rho_c$ is high (typically >0.1 Ω $cm^2$) based on the modified Ebers-Moll equivalent circuit analysis (see the circuit diagram in Figure 8).[68,69] The measured $\rho_c$ of Ca/Al was about 8 Ω $cm^2$ (see, Table 1). In case of a high $\rho_c$ value corresponding to the Ca/Al contacts, therefore, the overall cell output voltage is decreased because the voltage increase at the rear contact (oppositely directed Schottky diode) is larger than the voltage increase at the normal pn junction.

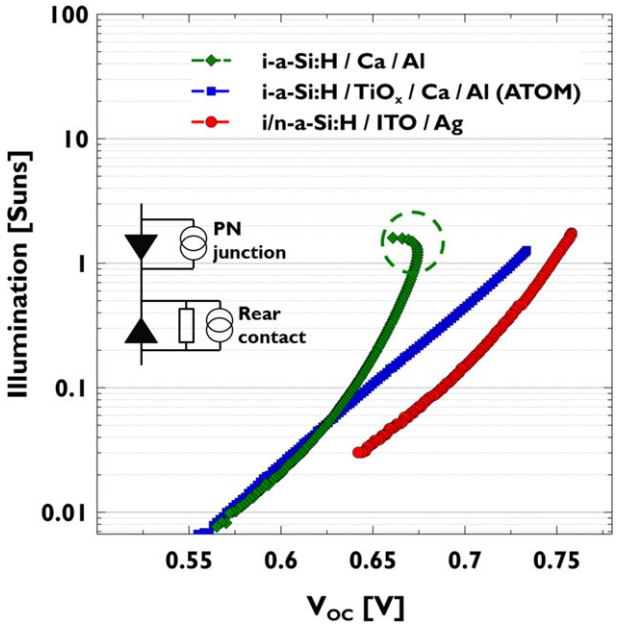


**FIGURE 8** Suns$V_{OC}$ measurements of the best solar cell in each group. The corresponding circuit diagram is the modified Ebers-Moll equivalent circuit including a Schottky diode in the rear contact.[68] The bend in the curves measured for both Al and Ca/Al contact is marked using a dashed circle [Colour figure can be viewed at wileyonlinelibrary.com]

Different a-Si:H properties after annealing a-Si:H with and without $TiO_x$ on the rear side might induce a large difference in $V_{OC}$ between the i-a-Si:H/Ca/Al contacted and the ATOM contacted solar cells. However, similar hydrogen contents of i-a-Si:H after belt furnace annealing at 175°C could be expected because of the very low effusion rate of an i-a-Si:H layer at annealing temperatures below 300°C.[70-73] Furthermore, the similar $J_0$ value in Table 1, the comparable EQE edge at the long wavelength range in Figure 7, and the overlapping Suns$V_{OC}$ curves at the low injection level in Figure 8 support a similar contact passivation quality of both the i-a-Si:H/Ca/Al and the ATOM contacts. Therefore, it can be seen that the low $\rho_c$ of the ATOM contact leads to high external $V_{OC}$.

On the other hand, the reference contact shows the highest $V_{OC}$ among the test groups because of the lower $J_{0,metal}$, typically below 10 fA/cm$^2$, and a strong field effect passivation. More downward band bending with a low $\rho_c$ should be aimed for to improve the electron-selective contact performance, which will be discussed after the FF analysis.

Because the performance of the various contact structures investigated in this work is very different in their $J_0$ and $\rho_c$ values, it is interesting to consider the FF losses in more detail as shown in Figure 9A. The series resistance of the solar cells is characterized using the Bowden method,[74] and the FF loss is outlined using the Khana method.[75] Generally, the FF can be expressed as:

$$FF = FF_{J01} - \Delta FF_{Rs} - \Delta FF_{Rsh} - \Delta FF_{J02} \quad (5)$$

where $FF_{J01}$ is the maximum attainable FF for the particular cell considering only $J_{01}$ recombination, $\Delta FF_{Rs}$ is the FF loss related to the series resistance of the solar cells as depicted in Figure 9B (including a $\rho_c$), $\Delta FF_{J02}$ is the FF loss resulting from $J_{02}$ recombination (the recombination in the space charge region), and $\Delta FF_{Rsh}$ is the FF loss associated with the shunt resistance of the solar cells. In all these cells, $\Delta FF_{Rsh}$ was only a very minor loss factor (0.01%-0.02%), so it is not considered in further detail here.

In the solar cells with i-a-Si:H/Ca/Al contacts, the sum of $FF_{Rs}$ and FF is already slightly higher (1%-2%) than $FF_{J01}$ because of the lower accuracy of the analysis in case of these solar cells because of the low FF value. Therefore, the $FF_{J02}$ values for the solar cells with i-a-Si:H/Ca/Al contacts are not mentioned in Figure 9A.

The very large $\Delta FF_{Rs}$ of 15% in the solar cell with an i-a-Si:H/Ca/Al rear contact can be significantly reduced by inserting the interfacial $TiO_x$ layer. The resulting performance of the ATOM contacts incorporating $TiO_x$ already yields a $\Delta FF_{Rs}$ below 10% and a $R_s$ close to 2 Ω cm$^2$, which approaches the values measured for the reference SHJ contact (i/n-a-Si:H/ITO/Ag). This FF analysis underlines that an

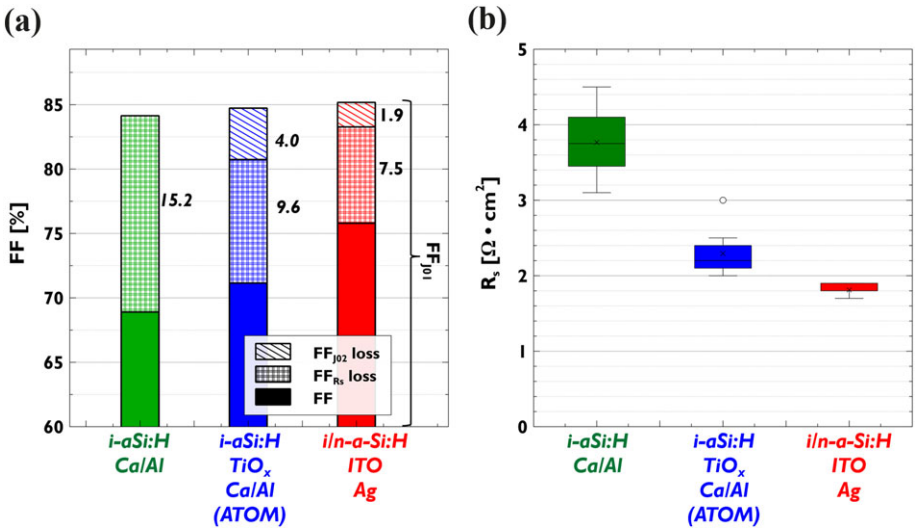


**FIGURE 9** FF, $FF_{J01}$, $\Delta FF_{Rs}$, and $\Delta FF_{J02}$ comparison (A) and dependence of the total series resistance of solar cells (B) on the type of metal rear contact. The $FF_{Rs}$ and $FF_{J02}$ losses are indicated in (A) [Colour figure can be viewed at wileyonlinelibrary.com]

**TABLE 3** Benchmarking the solar cell results for different passivating electron-selective contact structures

| Electron Contact Structure | Hole Contact Structure | $J_{SC}$ (mA/cm$^2$) | $V_{OC}$ (mV) | FF (%) | $\eta$ (%) |
|---|---|---|---|---|---|
| i-a-Si:H/TiO$_x$/Al[40] | i/p-a-Si:H/ITO/Ag | - | 677 | 54.0 | - |
| i-a-Si:H/TiO$_x$/ITO/Ag[40] | i/p-a-Si:H/ITO/Ag | - | 492 | 29.2 | - |
| i-a-Si:H/TiO$_x$/Al[78] | Boron diffused emitter/Cr/Pd/Ag | 40.5 | 570 | 57 | 13.2 |
| i-a-Si:H/TiO$_x$/Al/ITO/Ag[41] | i/p-a-Si:H/ITO/Ag | 35.5 | 612 | 71.3 | 15.5 |
| i-a-Si:H/TiO$_x$/Ca/Al (ATOM, this work) | i/p-a-Si:H/ITO/Ag | 35.1 | 711 | 72.9 | 18.2 |

added TiO$_x$ layer is strongly beneficial when aiming to make a passivating electron-selective contact based on a low work function metal to finally obtain acceptably low values for both $J_0$ and $\rho_c$.

However, the ATOM contact could not yet achieve higher performance than the conventional SHJ contact (i/n-a-Si:H/ITO/Ag). As can be seen in Figure 9A, the lower FF of the cells with the ATOM contact when compared to the reference can be mainly attributed to the higher $R_s$ and the larger recombination ($\Delta FF_{J02}$). Taking into account that all cells have the same front structure, the $R_s$ difference is caused by the rear contacts. The higher $R_s$ of the ATOM contacted cells compared to the reference cell might come from a higher $\rho_c$ resulting from the absence of an n-a-Si:H layer, or be induced by the much thinner rear metal than the printed Ag of the reference. In addition, without n-a-Si:H, and even with the TiO$_x$ and the Ca, the band bending seems to be reduced. Next to that, the thicker i-a-Si:H layer in the ATOM contact (8 nm instead of 4 nm in the reference contact) increases the probability of carrier recombination through the defect states in this layer.

Overall, to improve the ATOM contact performance, it is required to achieve a lower series resistance maintaining similar or lower $J_{0,metal}$ by forming more downward band bending at the electron contacts. The work of Matsui et al[76] demonstrated that the band bending could be tunable by the ALD TiO$_x$ growth conditions, likely because of the presence of fixed charge. Therefore, TiO$_x$ material development to control the fixed charge can be another alternative to enhance the band bending. Additionally, replacing the Ca with a lower work function metal could help to bend the bands further down to repel minority carriers more effectively. Possible materials here are again Sr or Yb ($\Phi$ = 2.4-2.5 eV instead of 2.9 eV for Ca[77]). These results are first cells demonstrating the ATOM contact, and there is room for further improvement.

In Table 3, the IV parameters for the best ATOM contact cells fabricated in this work are compared with previously reported results.[40,41,78] Especially, Ali et al[78] tested a-Si:H/TiO$_x$/Al contact in a boron diffused junction solar cell because of good contact passivation of a-Si:H/TiO$_x$ with respect to SiO$_x$/TiO$_x$. However, the cell performance was likely limited by a high contact resistivity and high anneal temperature of 350°C. In the work of Sacchetto et al,[41] a thin Al layer between TiO$_x$ and ITO was applied to form additional oxygen vacancies in the TiO$_x$ layer. However, it seems difficult to attain a good carrier selectivity[79] (a low $\rho_c$ and a low $J_{0,metal}$) by using TiO$_x$ with not sufficiently low work function metals on an i-a-Si:H passivation layer. As illustrated in this work, combining TiO$_x$ with a low work function metal such as Ca is an efficient route to decrease the $\rho_c$ and preserve a low $J_{0,metal}$, such that the $V_{OC}$ and FF values of the solar cells can be increased. Additionally, the low-temperature processing of the ATOM contact structure is compatible with the fabrication of hole-selective contacts based on high work function transition metal oxides.[33-39]

Finally, it has been reported that the quality of the Ca/Al electrode can be reduced because of the penetration of water through the pinholes in the capping layers.[80,81] Therefore, the stability improvement of ATOM contacts should also be a point of interest for future work.

## 4 | CONCLUSION

The ATOM contact structure including a TiO$_x$ layer and a low work function metal on an a-Si:H passivation layer was evaluated as a candidate for a passivating electron-selective contact for c-Si solar cells. Applying ALD-TiO$_x$ in the ATOM contact is an effective way to obtain a contact structure that combines good passivation properties with a low $\rho_c$. The integration of the ATOM contact into SHJ solar cells was successfully demonstrated and the best cell with an ATOM contact achieved a high $V_{OC}$ of 711 mV, a FF of 72.9%, $J_{SC}$ of 35.1 mA/cm$^2$, and an efficiency of 18.2%. However, the absence of a n-a-Si:H layer in the ATOM contact leads to losses in $V_{OC}$ and FF possibly caused by a weaker field effect passivation. These challenges may be overcome by applying a metal with a lower work function and possibly a higher reflectance than Ca, double side randomly textured substrates, improved i-a-Si:H passivation with thinner thickness, and the use of positively charged TiO$_x$ or extrinsically doped TiO$_x$.[82-87] Although the maximum efficiency of the ATOM contacted solar cell was lower than the more optimized conventional SHJ solar cell, the presented results indicate that the ATOM contact can pave the way toward highly efficient silicon solar cells without heavily doped Si layer.

## ACKNOWLEDGEMENTS

The authors gratefully acknowledge the financial support of imec's industrial affiliation program for Si-PV. Moreover, we would like to thank Arvid van der Heide and Monica Aleman for EQE reflectance measurements.

## ORCID

*Jinyoun Cho* http://orcid.org/0000-0002-3524-1256

## REFERENCES

1. Cho J, Shin HNR, Lee J, Choi Y, Lee J, Oh H, Kim T, Hwang M, Cho EC. 21%-efficient n-type rear-junction PERT solar cell with industrial thin 156mm Cz single crystalline silicon wafer, In *5h International Conference on Silicon Photovoltaic, SiliconPV 2015*, 2015. https://doi.org/10.1016/j.egypro.2015.07.039.

2. Urueña A, Aleman M, Cornagliotti E, et al. Progress on large area n-type silicon solar cells with front laser doping and a rear emitter.

*Progress in Photovoltaics: Research and Applications*. 2016;24(8):1149-1156. https://doi.org/10.1002/pip.2767

3. Ye F, Deng W, Guo W, Liu R, Chen D, Chen Y, Yang Y, Yuan N, Ding J, Feng Z, Altermatt PP, Verlinden PJ. 22.13% Efficient industrial p-type mono PERC solar cell, In *2016 IEEE 43rd Photovoltaic Specialists Conference (PVSC)*, IEEE; 2016.3360–3365. https://doi.org/10.1109/PVSC.2016.7750289.
4. Adachi D, Hernández JL, Yamamoto K. Impact of carrier recombination on fill factor for large area heterojunction crystalline silicon solar cell with 25.1% efficiency. *Appl Phys Lett*. 2015;107(23):233506. https://doi.org/10.1063/1.4937224
5. McIntosh KR, Altermatt PP, Ratcliff TJ, Fong KC, Black LE, Baker-Finch SC, Abbott MD. An examination of three common assumptions used to simulate recombination in heavily doped silicon, In 28th European Photovoltaic Solar Energy Conference and Exhibition, 2013.1672–1679. https://doi.org/128thEUPVSEC201/28thEUPVSEC2013-2CV.4.9
6. Holman ZC, Descoeudres A, Barraud L, et al. Current losses at the front of silicon heterojunction solar cells. *IEEE Journal of Photovoltaics*. 2012;2(1):7-15. https://doi.org/10.1109/JPHOTOV.2011.2174967
7. Melskens J, van de Loo BWH, Macco B, Vos MFJ, Palmans J, Smit S, Kessels WMM. Concepts and prospects of passivating contacts for crystalline silicon solar cells, In 2015 *IEEE 42nd Photovoltaic Specialist Conference (PVSC)*, IEEE; 2015. 1–6. https://doi.org/10.1109/PVSC.2015.7355646.
8. Melskens J, van de Loo BWH, Macco B, Black LE, Smit S, Kessels WMM. Passivating contacts for crystalline silicon solar cells: From concepts and materials to prospects. *IEEE Journal of Photovoltaics* 2018; 8: 1–16. https://doi.org/10.1109/JPHOTOV.2018.2797106, 2.
9. Schottky W. Halbleitertheorie der Sperrschicht. *Naturwissenschaften*. 1938;26(52):843-843. https://doi.org/10.1007/BF01774216
10. Mott NF. Note on the contact between a metal and an insulator or semi-conductor. *Mathematical Proceedings of the Cambridge Philosophical Society*. 1938;34(04):568. https://doi.org/10.1017/S0305004100020570
11. Allen TG, Bullock J, Zheng P, et al. Calcium contacts to n-type crystalline silicon solar cells. *Progress in Photovoltaics: Research and Applications*. 2016;25(7):636-644. https://doi.org/10.1002/pip.2838
12. Wan Y, Samundsett C, Yan D, et al. A magnesium/amorphous silicon passivating contact for n-type crystalline silicon solar cells. *Appl Phys Lett*. 2016;109(11):113901. https://doi.org/10.1063/1.4962960
13. Wan Y, Samundsett C, Bullock J, et al. Magnesium fluoride electron-selective contacts for crystalline silicon solar cells. *ACS Appl Mater Interfaces*. 2016;8(23):14671-14677. https://doi.org/10.1021/acsami.6b03599
14. Bullock J, Hettick M, Geissbühler J, et al. Efficient silicon solar cells with dopant-free asymmetric heterocontacts. *Nature Energy*. 2016;1(3):15031. https://doi.org/10.1038/nenergy.2015.31
15. Heine V. Theory of surface states. *Phys Rev*. 1965;138(6A):A1689-A1696. https://doi.org/10.1103/PhysRev.138.A1689
16. Sze SM, Ng KK. *Physics of semiconductor devices*. 3rd ed. Hoboken, NJ, USA: John Wiley & Sons; 2006:142-144.
17. Wronski CR, Carlson DE. Surface states and barrier heights of metal-amorphous silicon schottky barriers. *Solid State Commun*. 1977;23(7):421-424. https://doi.org/10.1016/0038-1098(77)90999-1
18. Mönch W. Mechanisms of Schottky-barrier formation in metal–semiconductor contacts. *J Vac Sci Technol B: Microelectronics and Nanometer Struct*. 1988;6(4):1270. https://doi.org/10.1116/1.584248
19. Mönch W. Electronic properties of ideal and interface-modified metal-semiconductor interfaces. *J Vac Sci Technol B*. 1996;14(4):2985-2993. https://doi.org/10.1116/1.588947
20. Paramahans Manik P, Kesh Mishra R, Pavan Kishore V, et al. Fermi-level unpinning and low resistivity in contacts to n-type Ge with a thin ZnO interfacial layer. *Appl Phys Lett*. 2012;101(18):1-6. https://doi.org/10.1063/1.4764909
21. Kobayashi M, Kinoshita A, Saraswat K, Wong H-SP, Nishi Y. Fermi level depinning in metal/Ge Schottky junction for metal source/drain Ge metal-oxide-semiconductor field-effect-transistor application. *J Appl Phys*. 2009;105(2):23702. https://doi.org/10.1063/1.3065990
22. King PJ, Arac E, Ganti S, Kwa KSK, Ponon N, O'Neill AG. Improving metal/semiconductor conductivity using AlOx interlayers on n-type and p-type Si. *Appl Phys Lett*. 2014;105(5):9-13. https://doi.org/10.1063/1.4892003
23. Hu J, Saraswat KC, Wong H-SP. Metal/III-V Schottky barrier height tuning for the design of nonalloyed III-V field-effect transistor source/drain contacts. *J Appl Phys*. 2010;107(6):63712. https://doi.org/10.1063/1.3327434
24. Kim J, Oldiges PJ, Li H, Niimi H, Raymond M, Zeitzoff P, Kamineni V, Adusumilli P, Chengyu Nui, Chafik F. Specific contact resistivity of n-type Si and Ge M-S and M-I-S contacts, In 2015 *International Conference on Simulation of Semiconductor Processes and Devices (SISPAD)*, Vol 2015–OctobIEEE; 2015.234–237. https://doi.org/10.1109/SISPAD.2015.7292302.
25. Yu H, Schaekers M, Barla K, et al. Contact resistivities of metal-insulator-semiconductor contacts and metal-semiconductor contacts. *Appl Phys Lett*. 2016;108(17):171602. https://doi.org/10.1063/1.4947580
26. Avasthi S, McClain WE, Man G, Kahn A, Schwartz J, Sturm JC. Hole-blocking titanium-oxide/silicon heterojunction and its application to photovoltaics. *Appl Phys Lett*. 2013;102(20):9-13. https://doi.org/10.1063/1.4803446
27. Agrawal A, Lin J, Zheng B, Sharma S, Chopra S, Wang K, Gelatos A, Mohney S, Datta S. Barrier height reduction to 0.15eV and contact resistivity reduction to 9.1×10−9 Ω-cm2 using ultrathin TiO2−x interlayer between metal and silicon, In 2013 Symposium on VLSI Technology (VLSIT), 2013. T200–T201.
28. Remesh N, Dev S, Rawal Y, Khopkar S, Manik PP, Wood B, Brand A, Lodha S. Contact barrier height and resistivity reduction using low work-function metal (Yb)-interfacial layer-semiconductor contacts on n-type Si and Ge, In 2015 73rd Annual Device Research Conference (DRC), IEEE; 2015.145–146. https://doi.org/10.1109/DRC.2015.7175597.
29. Agrawal A, Lin J, Barth M, et al. Fermi level depinning and contact resistivity reduction using a reduced titania interlayer in n-silicon metal-insulator-semiconductor ohmic contacts. *Appl Phys Lett*. 2014;104(11):112101. https://doi.org/10.1063/1.4868302
30. Yang X, Zheng P, Bi Q, Weber K. Silicon heterojunction solar cells with electron selective TiOx contact. *Solar Energy Materials and Solar Cells*. 2016;150:32-38. https://doi.org/10.1016/j.solmat.2016.01.020
31. Yang X, Bi Q, Ali H, Davis K, Schoenfeld WV, Weber K. High-performance TiO2-based electron-selective contacts for crystalline silicon solar cells. *Adv Mater*. 2016;28(28):5891-5897. https://doi.org/10.1002/adma.201600926
32. Yang X, Weber K, Hameiri Z, De Wolf S. Industrially feasible, dopant-free, carrier-selective contacts for high-efficiency silicon solar cells. *Progress in Photovoltaics: Res Appl*. 2017;25(11):896-904. https://doi.org/10.1002/pip.2901
33. Bullock J, Cuevas A, Allen T, Battaglia C. Molybdenum oxide MoOx: A versatile hole contact for silicon solar cells. *Appl Phys Lett*. 2014;105(23):232109. https://doi.org/10.1063/1.4903467
34. Battaglia C, Yin X, Zheng M, et al. Hole selective MoOx contact for silicon solar cells. *Nano Lett*. 2014;14(2):967-971. https://doi.org/10.1021/nl404389u
35. Almora O, Gerling LG, Voz C, Alcubilla R, Puigdollers J, Garcia-Belmonte G. Superior performance of V2O5 as hole selective contact over other transition metal oxides in silicon heterojunction solar cells. *Solar Energy Materials and Solar Cells*. 2017;168:221-226. https://doi.org/10.1016/j.solmat.2017.04.042
36. Macco B, Vos MFJ, Thissen NFW, Bol AA, Kessels WMM. Low-temperature atomic layer deposition of MoOx for silicon heterojunction solar cells. *Physica Status Solidi (RRL) - Rapid Res Lett*. 2015;9(7):393-396. https://doi.org/10.1002/pssr.201510117

37. Geissbühler J, Werner J, Martin De Nicolas S, et al. 22.5% efficient silicon heterojunction solar cell with molybdenum oxide hole collector. *Appl Phys Lett*. 2015;107(8):81601. https://doi.org/10.1063/1.4928747

38. Gerling LG, Mahato S, Morales-Vilches A, et al. Transition metal oxides as hole-selective contacts in silicon heterojunctions solar cells. *Solar Energy Mat and Solar Cells*. 2016;145:109-115. https://doi.org/10.1016/j.solmat.2015.08.028

39. Gerling LG, Voz C, Alcubilla R, Puigdollers J. Origin of passivation in hole-selective transition metal oxides for crystalline silicon heterojunction solar cells. *J Mat Res*. 2017;32(02):260-268. https://doi.org/10.1557/jmr.2016.453

40. Boccard M, Yang X, Weber K, Holman ZC. Passivation and carrier selectivity of TiO2 contacts combined with different passivation layers and electrodes for silicon solar cells, in 2016 *IEEE 43rd Photovoltaic Specialists Conference (PVSC)*, Vol 2016–NovemIEEE; 2016.2403–2407. https://doi.org/10.1109/PVSC.2016.7750072.

41. Sacchetto D, Jeangros Q, Christmann G, Barraud L, Descoeudres A, Geissbuhler J, Despeisse M, Hessler-Wyser A, Nicolay S, Balllif C. MoOx and TiO2 carrier selective contacts for dopant-free SHJs, In *7th International Conference on Crystalline Silicon Photovoltaics 2017*, 2017.

42. Cho J, Debucquoy M, Payo MR, Malik S, Filipic M, Sivaramakrishnan Radhakrishnan H, Bearda T, Gordon I, Szlufcik J, Poortmans J. Contact resistivity reduction on lowly-doped n-type Si using a low workfunction metal and a thin TiOx interfacial layer for doping-free Si solar cells, In *7th International Conference on Silicon Photovoltaic, SiliconPV 2017*, 2017. https://doi.org/10.1016/j.egypro.2017.09.356, 842, 850.

43. Kopp J, Warta W, Aberle A, Glunz S, Knobloch J. Impact of metallization techniques on 20% efficient silicon solar cells, In 22nd IEEE Photovoltaic Specialists Conference, 1991.278–283. https://doi.org/10.1109/PVSC.1991.169224

44. Klaver A. Irradiation-induced degradation of amorphous silicon solar cells in space. Delft Univeristy of Dent Technology, 2007.

45. Sinton RA, Cuevas A. Contactless determination of current–voltage characteristics and minority-carrier lifetimes in semiconductors from quasi-steady-state photoconductance data. *Appl Phys Lett*. 1996;69(17):2510-2512. https://doi.org/10.1063/1.117723

46. Street RA. *Hydrogenated amorphous silicon*. Cambridge: Cambridge University Press; 1991:321-322.

47. Hunter MS, Fowle P. Natural and thermally formed oxide films on aluminum. *J Electrochem Soc*. 1956;103(9):482. https://doi.org/10.1149/1.2430389

48. Dumas P, Rivi D, Levy Y, Corset J, Dumas P, Rivi D. Growth of thin alumina film on aluminum at room temperature: A kinetic and spectroscopic study by surface plasmon excitation. *Le Journal de Physique Colloques*. 1983;44:C10–205-C10–208. https://doi.org/10.1051/jphyscol:19831042

49. Franklin E, Fong K, McIntosh K, et al. Design, fabrication and characterisation of a 24.4% efficient interdigitated back contact solar cell. *Prog in Photovoltaics: Res Appl*. 2016;24(4):411-427. https://doi.org/10.1002/pip.2556

50. Liu Y, Chen Y, LaFehr DT, Su Y, Huo Y, Kang Y, Deng H, Jia J, Zhao L, Yuan M, Lyu Z, De Witt D, Vilgalys MA, Zang K, Chen X, Lu C-Y, Kamins TI, Harris JS. Titanium oxide electron-selective layers for contact passivation of thin-film crystalline silicon solar cells, In: Teherani FH, Look DC, Rogers DJ, editors. In *SPIE Proceedings Vol. 9749*, SPIE; 2016. 97491J. https://doi.org/10.1117/12.2213540.

51. Cuevas A, Basore PA, Giroult-Matlakowski G, Dubois C. Surface recombination velocity of highly doped n -type silicon. *J Appl Phys*. 1996;80(6):3370-3375. https://doi.org/10.1063/1.363250

52. Schroder DK. Semiconductor material and device characterization, Third Edition. vol. 44 Hoboken, NJ, USA: John Wiley & Sons, Inc.; 2005.135–136.

53. Abdulraheem Y, Gordon I, Bearda T, Meddeb H, Poortmans J. Optical bandgap of ultra-thin amorphous silicon films deposited on crystalline silicon by PECVD. *AIP Adv*. 2014;4(5):57122. https://doi.org/10.1063/1.4879807

54. Meddeb H, Bearda T, Abdelraheem Y, et al. Structural, hydrogen bonding and in situ studies of the effect of hydrogen dilution on the passivation by amorphous silicon of n-type crystalline (1 0 0) silicon surfaces. *J Phys D Appl Phys*. 2015;48(41):415301. https://doi.org/10.1088/0022-3727/48/41/415301

55. Yu I-S, Chang I-H, Cheng H-E, Lin Y-S. Surface passivation of c-Si by atomic layer deposition TiO2 thin films deposited at low temperature, In 2014 IEEE 40th Photovoltaic Specialist Conference (PVSC), IEEE; 2014.1271–1274. https://doi.org/10.1109/PVSC.2014.6925148.

56. Kita K, Toriumi A. Origin of electric dipoles formed at high-k/SiO2 interface. *Appl Phys Lett*. 2009;94(13):132902. https://doi.org/10.1063/1.3110968

57. Allen TG, Bullock J, Jeangros Q, et al. A low resistance calcium/reduced titania passivated contact for high efficiency crystalline silicon solar cells. *Adv Energy Mat*. 2017;7(12):1602606. https://doi.org/10.1002/aenm.201602606

58. Roose B, Pathak S, Steiner U. Doping of TiO2 for sensitized solar cells. *Chem Soc Rev*. 2015;44(22):8326-8349. https://doi.org/10.1039/c5cs00352k

59. Ali H, Yang X, Davis KO, Weber K, Schoenfeld WV. TEM studies of TiO2-based passivated contacts in c-Si solar cells. *Microsc Microanal*. 2016;22(S3):1600-1601. https://doi.org/10.1017/S1431927616008849

60. Zhang Y, Yu C, Yang M, et al. Optimization of the window layer in large area silicon heterojunction solar cells. *RSC Adv*. 2017;7(15):9258-9263. https://doi.org/10.1039/C6RA26342A

61. Chang CY, Fang YK, Sze SM. Specific contact resistance of metal-semiconductor barriers. *Solid State Electron*. 1971;14(7):541-550. https://doi.org/10.1016/0038-1101%20(71)90129-8

62. Ng KK, Wiley AJ. *Physics of devices semiconductor*. Third ed.; n.d.

63. Haslinger M, Soha M, Jambaldinni S, Hajjiah A, Szlufcik J, Poortmans J, John J. Novel wet chemical cleaning concepts for high efficiency silicon solar cells. In 33rd European Photovoltaic Solar Energy Conference and Exhibition 2017; 628–630.

64. Greiner MT, Lu Z. Thin-film metal oxides in organic semiconductor devices: Their electronic structures, work functions and interfaces. *NPG Asia Mat*. 2013;5(7):e55. https://doi.org/10.1038/am.2013.29

65. Endriz JG, Spicer WE. Reflectance studies of Ba, Sr, Eu, and Yb. *Phys Rev B*. 1970;2(6):1466-1492. https://doi.org/10.1103/PhysRevB.2.1466

66. Ehrenreich H, Philipp HR, Segall B. Optical properties of aluminum. *Phys Rev*. 1963;132(5):1918-1928. https://doi.org/10.1103/PhysRev.132.1918

67. Pandey AK, Shaw PE, Samuel IDW, Nunzi J-M. Effect of metal cathode reflectance on the exciton-dissociation efficiency in heterojunction organic solar cells. *Appl Phys Lett*. 2009;94(10):103303. https://doi.org/10.1063/1.3098472

68. Green MA, Blakers AW, Zhao J, Milne AM, Wang A, Dai X. Characterization of 23-percent efficient silicon solar cells. *IEEE Trans on Electron Dev*. 1990;37(2):331-336. https://doi.org/10.1109/16.46361

69. Glunz SW, Nekarda J, Mäckel H, Cuevas A. Analyzing back contacts of silicon solar cells by Suns-Voc-measurements at high illumination densities, In Proceedings of the 22nd European Photovoltaic Solar Energy Conference 2007.849–853.

70. De Wolf S, Kondo M. Nature of doped a-Si:H/c-Si interface recombination. *J Appl Phys*. 2009;105(10):103707. https://doi.org/10.1063/1.3129578

71. Melskens J, Smets AHMM, Schouten M, Eijt SWHH, Schut H, Zeman M. New insights in the nanostructure and defect states of hydrogenated amorphous silicon obtained by annealing. *IEEE J Photovoltaics*. 2013;3(1):65-71. https://doi.org/10.1109/JPHOTOV.2012.2226870

72. Melskens J, Eijt SWHH, Schouten M, et al. Migration of open volume deficiencies in hydrogenated amorphous silicon during annealing. *IEEE J Photovoltaics*. 2017;7(2):421-429. https://doi.org/10.1109/JPHOTOV.2016.2646421
73. Beyer W. Hydrogen effusion: A probe for surface desorption and diffusion. *Physica B: Physics of Condensed Matter*. 1991;170(1-4):105-114. https://doi.org/10.1016/0921-4526%20(91)90111-Q
74. Bowden S, Rohatgi A. Rapid and accurate determination of series resistance and fill factor losses in industrial silicon solar cells, In *17th European Photovoltaic Solar Energy Conference and Exhibition* 2001.
75. Khanna T, Stangl B, Basu PK, et al. Fill factor loss analysis method for silicon wafer solar cells. *IEEE Journal of Photovoltaics*. 2013;3(4):1170-1177. https://doi.org/10.1109/JPHOTOV.2013.2270348
76. Matsui T, Bivour M, Ndione P, Hettich P, Hermle M. Investigation of atomic-layer-deposited TiOx as selective electron and hole contacts to crystalline silicon, In *7th International Conference on Silicon Photovoltaic, SiliconPV 2017*, 2017. https://doi.org/10.1016/j.egypro.2017.09.093, 628, 634.
77. Skriver HL, Rosengaard NM. Surface energy and work function of elemental metals. *Phys Rev B*. 1992;46(11):7157-7168. https://doi.org/10.1103/PhysRevB.46.7157
78. Ali H, Yang X, Weber K, Schoenfeld WV, Davis KO. Transmission electron microscopy studies of electron-selective titanium oxide contacts in silicon solar cells. *Microsc Microanal*. 2017;23(05):1-5. https://doi.org/10.1017/S1431927617012417
79. Brendel R, Rienaecker M, Peibst R. A quantitative measure for the carrier selectivity of contacts to solar cells, In 32nd European Photovoltaic Solar Energy Conference and Exhibition, 2016.2–6. https://doi.org/10.4229/EUPVSEC20162016-2CO.4.1
80. Keuning W, van de Weijer P, Lifka H, Kessels WMM, Creatore M. Cathode encapsulation of organic light emitting diodes by atomic layer deposited Al2O3 films and Al2O3/a-SiNx:H stacks. *J Vac Sci Technol a*. 2012;30(1):01A131. https://doi.org/10.1116/1.3664762
81. Park JS, Chae H, Chung HK, Lee SI. Thin film encapsulation for flexible AM-OLED: A review. *Semiconductor Science and Technology*. 2011;26(3):034001. https://doi.org/10.1088/0268-1242/26/3/034001
82. Nikolay T, Larina L, Shevaleevskiy O, Ahn BT. Electronic structure study of lightly Nb-doped TiO2 electrode for dye-sensitized solar cells. *Energ Environ Sci*. 2011;4(4):1480. https://doi.org/10.1039/c0ee00678e
83. Tsvetkov N, Larina L, Shevaleevskiy O, Ahn BT. Effect of Nb doping of TiO2 electrode on charge transport in dye-sensitized solar cells. *J Electrochem Soc*. 2011;158(11):B1281. https://doi.org/10.1149/2.010111jes
84. Furubayashi Y, Hitosugi T, Yamamoto Y, et al. Transparent metal: Nb-doped anatase TiO2. *Appl Phys Lett*. 2005;86(25):1-3. https://doi.org/10.1063/1.1949728
85. Niu Z, Gao F, Jia X, Zhang W, Chen W, Qian K. Synthesis studies of sputtering TiO2 films on poly (dimethylsiloxane) for surface modification. *Colloids Surf a Physicochem Eng Asp*. 2006;272(3):170-175. https://doi.org/10.1016/j.colsurfa.2005.07.024
86. Mazzolini P, Russo V, Casari CS, et al. Vibrational-electrical properties relationship in donor-doped TiO2 by Raman spectroscopy. *J Phys Chem C*. 2016;120(33):18878-18886. https://doi.org/10.1021/acs.jpcc.6b05282
87. Hitosugi T, Furubayashi Y, Ueda A, et al. Ta-doped Anatase TiO2 epitaxial film as transparent conducting oxide. *Jpn J Appl Phys*. 2005;44(34):L1063-L1065. https://doi.org/10.1143/JJAP.44.L1063

## SUPPORTING INFORMATION

Additional supporting information may be found online in the Supporting Information section at the end of the article.

**How to cite this article:** Cho J, Melskens J, Debucquoy M, et al. Passivating electron-selective contacts for silicon solar cells based on an a-Si:H/$TiO_x$ stack and a low work function metal. *Prog Photovolt Res Appl*. 2018;26:835–845. https://doi.org/10.1002/pip.3023